

# Supporting Information

## Single Nanoparticle Nitrogen Dioxide Gas Sensor Using Active Molecular Plasmonics

Lichan Chen, Bo Wu, Longhua Guo, Ruiwen Tey, Youju Huang, Dong-Hwan Kim\*

School of Chemical and Biomedical Engineering, Nanyang Technological University,

70 Nanyang Drive, Singapore 637457, Singapore

\*e-mail: [dhkim@ntu.edu.sg](mailto:dhkim@ntu.edu.sg) (Dong-Hwan Kim)

## Experimental Section

**Chemicals.** Hydrogen tetrachloroaurate(III) trihydrate ( $\text{HAuCl}_4 \cdot 3\text{H}_2\text{O}$ ), Cetyltrimethylammonium bromide (CTAB), sodium borohydride ( $\text{NaBH}_4$ ), ascorbic acid, silver nitrate ( $\text{AgNO}_3$ ), 11-(Ferrocenyl)undecanethiol ( $\text{FcC}_{11}\text{SH}$ ), acetonitrile, sodium hydroxide ( $\text{NaOH}$ ), and 5A molecular sieves were purchased from Sigma-Aldrich. Molecular sieves was activated and used for drying acetonitrile, according to a previously reported method.<sup>1</sup> Polydimethylsiloxane (PDMS, Sylgard 184) was purchased from Dow Corning.  $\text{CO}_2$  was supplied by National Oxygen Pte Ltd (Singapore) and other gas samples were prepared in our lab.  $\text{NO}_2$  standard gases with various concentrations were prepared by diluting 1%  $\text{NO}_2$  gas with appropriate volumes of simulated air, i.e. the gas mixture of  $\text{O}_2$  and  $\text{N}_2$  with 1:4 volume ratios. All experiments were carried out at room temperature ( $25 \pm 1$  °C).

**Synthesis of Au nanorods.** The Au NRs with a longitudinal plasmon resonance wavelength of 660 nm were synthesized by overgrowing a starting Au NRs (a longitudinal plasmon resonance wavelength of 774 nm) according to the previous reports.<sup>2-4</sup> For the growth of the starting Au NRs sample, a seed solution was prepared by adding a freshly prepared, ice cold  $\text{NaBH}_4$  (0.6 mL, 0.01 M) into a mixture of CTAB (5 mL, 0.2 M) and  $\text{HAuCl}_4$  (5 mL, 0.5 mM) under vigorous stirring and maintained stirring for 2 min. After stirring, the obtained brownish yellow seed solution was kept at 25 °C for at least 10 min before use. A growth solution was made by the sequential addition of  $\text{HAuCl}_4$  (2.5 mL, 0.01 M),  $\text{AgNO}_3$  (300  $\mu\text{L}$ , 0.01M) and ascorbic acid (275  $\mu\text{L}$ , 0.1 M) into CTAB (47.5 mL, 0.1 M). After the resultant solution was stirred for 2 min, 60  $\mu\text{L}$  of as-prepared seed solution was added. The mixture was again vigorously stirred for 20 s and then left undisturbed at least overnight. The twice-centrifuged (7000 rpm, 20 min) starting Au NRs were subjected

to the overgrowth by adding 200  $\mu\text{L}$  of the as-prepared starting AuNR solution into 10 mL of the growth solution consisting of 0.01 M CTAB, 0.25 mM  $\text{HAuCl}_4$ , 0.01 M ascorbic acid. The mixture solution was gently stirred for 2 min, followed by keeping at 30  $^\circ\text{C}$  in a water bath for at least 12 h. Absorption spectra were recorded with a Shimadzu UV-2450 spectrophotometer. The size and morphology of the synthesized AuNRs were obtained by the JEOL instrument (JSM-6700F) at an acceleration voltage of 5 kV and a working distance of 7-8 mm.

**Fabrication of the double layer microfluidic chip.** The microfluidic chip consists of four components, including a bottom glass substrate, a fluidic-channel PDMS layer, an air-channel PDMS layer and a top glass cover (Fig. 1E). The two PDMS layers were made by standard soft-lithography technique. Firstly, the molds of fluidic-channel PDMS layer and air-channel PDMS layer were made on silicon wafers by photolithography of negative photoresist (SU-8 2015, MicroChem, USA) in height of 20  $\mu\text{m}$ . To peel off the cured PDMS from the molds easily, the molds were treated with carbon tetrafluoride ( $\text{CF}_4$ ). Secondly, the two PDMS layers were templated from their molds. Spin coating was used to precisely control the thickness of PDMS layers. For the fluidic-channel layer, PDMS precursor was prepared by mixing PDMS base and its curing agent in ratio of 20:1. The degassed PDMS precursor was poured on the fluidic-channel mold and spin coated over the mold at speed of 600 rpm for 5 min. The cured fluidic-channel PDMS layer was made in the thickness of 25  $\mu\text{m}$ . For the air-channel layer, PDMS precursor was prepared by mixing PDMS base and its curing agent in ratio of 5:1. The air-channel layer was made in thickness of 600  $\mu\text{m}$  by spin coating at speed of 60 rpm for 5 min. After heating on a hot plate at 80  $^\circ\text{C}$  for 30 min, the semi-cured air-channel PDMS layer was peeled off from its mold and placed on the semi-cured fluidic-network layer with

alignment. The diffusion of curing agent from the air-channel layer to the fluidic-channel layer forms a reliable bonding by heating for another 3 hours. Then the bonded PDMS structure was peeled off from the fluidic-channel mold, punched with holes as inlets and outlets and bonded on a glass substrate (75 mm × 25 mm × 0.1 mm) by oxygen plasma. To prevent the PDMS structure from swelling by absorbing silicon oil used for the oil-immersion light condenser of dark-field microscope, the centre area of PDMS structure was covered with a square thin glass slide (22 mm × 22 mm × 0.1 mm). The microfluidic chip was held on the dark-field microscope by an acrylic frame cut by CO<sub>2</sub> laser. HPLC fittings were used as macro-micro interfaces to infuse reagents into the thin microfluidic chip without leakage.

**Au NRs immobilization.** In a typical run, the experiment was carried out as the following steps: (1) to activate the surface of the glass substrate, an aqueous NaOH (2.0 M) solution was injected into the fluidic-channel and incubated for 20 min to generate a dense layer of negative charges on the glass substrate.<sup>5</sup> The channel was rinsed thoroughly with distilled water. (2) To immobilize the Au NRs, an Au NRs suspension 10-fold diluted with 6.25 mM CTAB solution was passed through the fluidic-channel and incubated for 5 min.<sup>6</sup> The channel was rinsed with distilled water, and then with acetonitrile. (3) After each cycle of detection, the fluidic-channel was rinsed with a diluted potassium iodide solution (gold etchant type TFA (Transene Company Inc.): H<sub>2</sub>O = 1:4 (v/v)) for 1 min to effectively remove the layer of Au NRs.<sup>5</sup> The fluidic-channel could be re-activated with 2.0 M NaOH, and another cycle of Au NRs immobilization could be conducted as described above.

**Single nanoparticle DFM imaging and scattering spectroscopy.** Dark field imaging and spectroscopy on single Au nanorods (NRs) were carried out on Olympus IX71 inverted microscope coupled with an oil immersion dark-field condenser

( $1.2 < \text{NA} < 1.4$ ), a motorized stage (Ludl Flat-top inverted stage 96S106-N3-LE2, BioVision Technologies), a color digital camera (DS-Fi1-U2 with the NIS Element D software), and a line-imaging spectrometer (Acton Research SpectraPro2150i with a grating of 300 lines/mm) with a cooled spectrograph CCD camera ( $1340 \times 100$  pixel and pixel size of  $20\mu\text{m}$ ). More details of the dark-field microscopy and spectroscopy setup have been reported in our previous work.<sup>7</sup> After the AuNR-functionalized microfluidic chip was mounted on the microscope stage, the area in the center of microfluidic channel with uniform AuNRs distribution was selected as the region of interest. After proper focusing of the condenser and the objective, the true-color scattering images of AuNRs were taken using a  $100\times$  oil immersion Plan Semi Apochromat objective (NA 0.6-1.3) and the true-color digital camera with a white light illumination from a 100 W halogen lamp. The scattering spectra of AuNR were routed to spectrograph CCD. The slit that was internally mounted on the spectrometer entrance was set to  $20\ \mu\text{m}$  to match the size of a single pixel of the cooled spectrograph CCD camera for imaging reconstruction. The spectrum library of AuNRs was captured by scanning a  $20\ \mu\text{m} \times 20\ \mu\text{m}$  area of the AuNR functionalized microfluidic channel, using the motorized stage and the spectrometer coupled to the CCD camera. Combined with a systematically assembled darkfield platform, our customized synchronization software could map spectrum intensities of nanoparticles onto a reconstructed image. On the basis of one-to-one correspondence between a true-color scattering image and a black-to-white, reconstructed pseudoimage, the LSPR spectrum of each particle could be simply retraced. The spectra were fitted by a Lorentzian function using Origin program for accurate determination of  $\lambda_{\text{max}}$ .

**Gas Sensing.** After the immobilization of Au NRs in the channel, a solution containing 5 mM FcC<sub>11</sub>SH in acetonitrile was injected into the fluidic-channel and

incubated for 3 h to form a dense, self-assembled monolayer of  $\text{FcC}_{11}\text{SH}$ . The channel was then rinsed with acetonitrile to remove excess  $\text{FcC}_{11}\text{SH}$ . Then,  $\text{NO}_2$  gas sample was introduced into the air-channel for 15 min at the flow rate of  $0.1 \text{ mL min}^{-1}$ . The air-channel was then injected with acetonitrile. The LSPR spectra were monitored before and after gas injection. Notably, thorough drying both a target gas mixture and an acetonitrile solution is necessary prior to testing because in the presence of water, a nitric acid would be formed, which may etch AuNRs,<sup>8</sup> causing changes in the scattering profiles. The flow rate of the gas mixtures and the fluids were controlled by a syringe pump (KDS 210, KD Scientific, US).

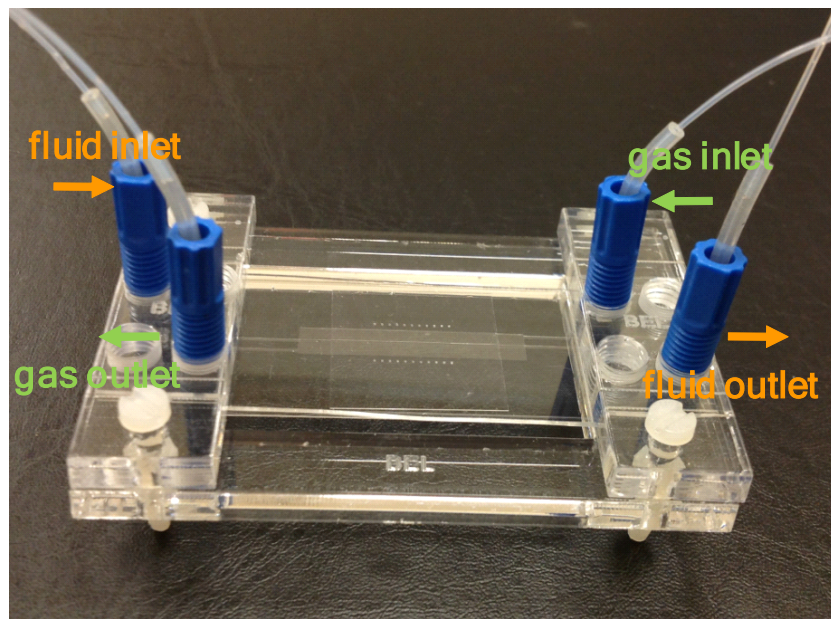


Figure S1. Image showing the location of the sensor pads on an actual device, as well as the inlet and outlet locations for fluid and gas flow (arrows).

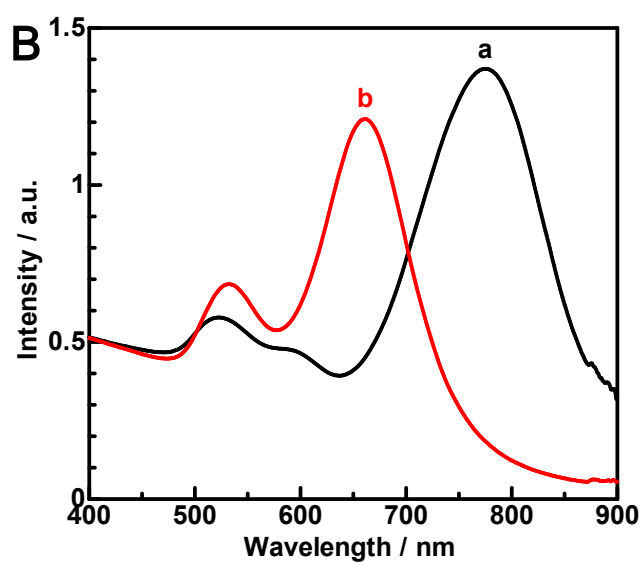
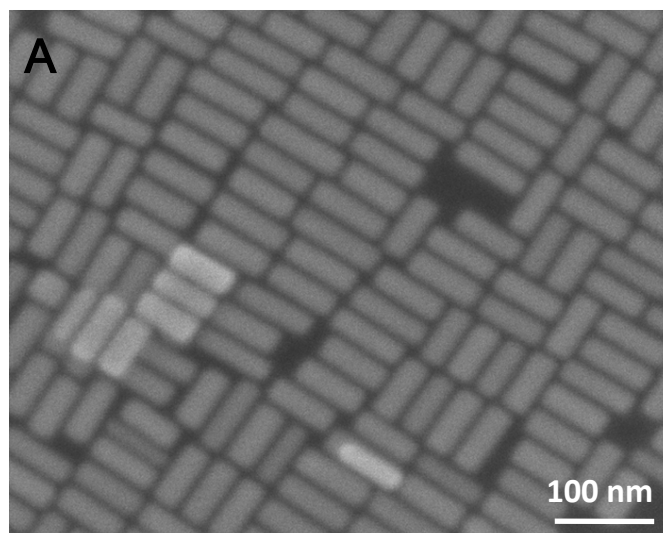


Figure S2. (A) SEM image of AuNR seeds before tip overgrowth. (B) UV-vis spectra of (a) AuNR seeds, (b) overgrown AuNRs to tune their LSPR peak to 665 nm.

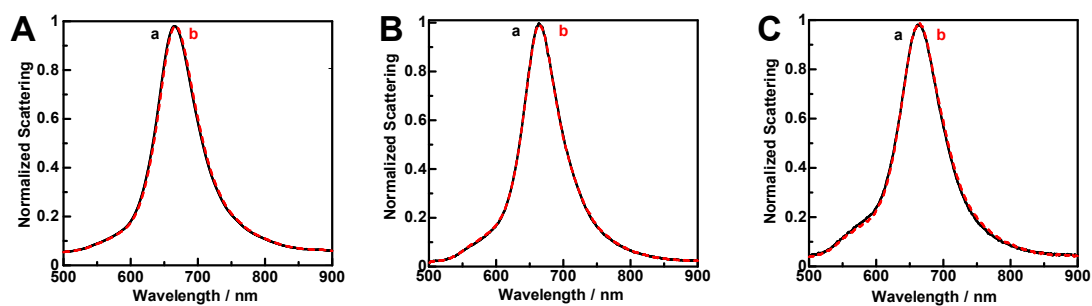


Figure S3. Steady-state LSPR spectra recorded from (A) a bare AuNR in acetonitrile with peak wavelength of 665.70 nm upon injection of 2000 ppm NO<sub>2</sub> gas; (B) a 6-mercaptohexanol-modified AuNR in acetonitrile with peak wavelength of 665.0 nm upon injection of 2000 ppm NO<sub>2</sub> gas; (C) a ferrocene-modified AuNR in acetonitrile with peak wavelength of 664.7 nm upon the injection of pure N<sub>2</sub> gas.

### **Other probable factors that contribute to the spectral shift in the event of NO<sub>2</sub> injection:**

Upon the injection of analyte, NO<sub>2</sub>, the scattering peak red-shifted by 4.87 nm from 665.28 to 670.15 nm. In addition to the refractive index change resulted from the oxidation of ferrocene to ferrocenium other probable factors that contribute to the spectral shift include followings. First, surface plasmon-enhanced molecular absorption and plasmonic-molecular resonance coupling provide positive contribution. When the longitudinal plasmon peak of AuNR overlaps with the absorption wavelength of resonance molecule, the molecule-surface plasmon interaction gives rise to plasmonic coupling. In this quantum regime, the photon is continuously exchanged between the molecules and the localized plasmons, resulting in the hybridization of molecular absorption and plasmon resonance and thus the splitting of the surface plasmon modes, in which coupling-induced red plasmon shift can be observed.<sup>9-11</sup> Second, oxidation-induced orientation changes of FcC11SH SAM exhibit certain negative contribution. The oxidation of ferrocene to ferrocenium introduces two kinds of electrostatic repulsions, i.e., that between two adjacent ferrocenium cations and that between the positively charged AuNR and the ferrocenium cation. To offset the electrostatic repulsions, the angle between ferrocene and the alkyl chain would decrease with respect to the surface normal,<sup>12</sup> and rotation/flipping of the Fc group around the alkyl chain would occur.<sup>13</sup> As reported previously,<sup>14, 15</sup> the FcC11SH molecular reorganization not only increases the monolayer thickness but also decreases the refractive index value of the monolayer by incorporating more solvent molecules into the monolayer, resulting in the blue-shift. Third, a decrease in the number of free electrons resulted from the formation of positively charged ferrocenium gives rise to positive contribution. It has been proved that the longitudinal plasmon wavelength of AuNR can be strongly affected by the change in the electron density.<sup>16</sup> A decrease in the number of free electrons will result in a red shift of the plasmon resonance due to the reduced restoring force, vice versa.<sup>17</sup>

### The effect of the concentration of NO<sub>2</sub> on the ferrocene oxidation:

It is well-known that ferrocene is a most widely used redox probe that easily undergoes one electron oxidation to form ferricenium cation in a reversible manner. In cyclic voltammetry (CV), the oxidation peak current ( $i_p$ ) of ferrocene generally follows Randles-Sevcik equation:

$$i_p = 2.69 \times 10^5 n^{3/2} A D^{1/2} C v^{1/2}$$

Where  $n=1$ ;  $A$  is the surface area of the working electrode;  $D$  is the diffusion coefficient of ferrocene;  $C$  is the bulk concentration of ferrocene; and  $v$  is the scan rate of voltammograms. For a given electrochemical system,  $A$ ,  $D$ , and  $v$  can all be constants, and thus  $i_p$  is proportional to the bulk concentration of ferrocene. Therefore, NO<sub>2</sub>-induced ferrocene oxidation followed by CV measurement can be used for monitoring the effect of NO<sub>2</sub> concentration on the ferrocene oxidation. It was expected that  $i_p$  would decrease with the increase of NO<sub>2</sub> concentration due to NO<sub>2</sub>-induced ferrocene consumption. In the CV experiment, glassy carbon electrode (2 mm in diameter), Pt wire and Ag wire was used as working electrode, counter electrode, and reference electrode, respectively. 1 mL acetonitrile containing 0.1 M tetrabutylammonium hexafluorophosphate and 1 mM ferrocene was used as a testing solution. CVs in the potential range of -0.3 - 0.3V were measured once 10 mL of different concentrations of NO<sub>2</sub> have been passed through the testing solution at a fixed flow rate (300 mL h<sup>-1</sup>). A decrease in  $i_p$  were indeed observed by increasing NO<sub>2</sub> concentration from 1 to 1000 ppm, as shown in Fig.S4.

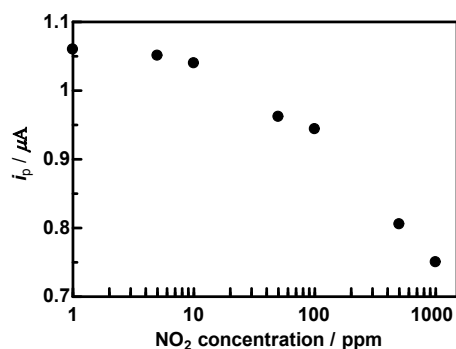


Figure S4. The oxidation peak current ( $i_p$ ) of 1 mM ferrocene as a function of the

concentration of NO<sub>2</sub>.

## References

1. P. J. Welford, B. A. Brookes, J. D. Wadhawan, H. B. McPeak, C. E. W. Hahn and R. G. Compton, *J. Phys. Chem. B*, 2001, **105**, 5253-5261.
2. B. Nikoobakht and M. A. El-Sayed, *Chem. Mater.*, 2003, **15**, 1957-1962.
3. K. Sohn, F. Kim, K. C. Pradel, J. Wu, Y. Peng, F. Zhou and J. Huang, *ACS Nano*, 2009, **3**, 2191-2198.
4. Y. Huang, A. R. Ferhan and D.-H. Kim, *Nanoscale*, 2013, **5**, 7772-7775.
5. L. Guo, Y. Huang, Y. Kikutani, Y. Tanaka, T. Kitamori and D.-H. Kim, *Lab on a Chip*, 2011, **11**, 3299-3304.
6. L. Guo, X. Zhou and D.-H. Kim, *Biosens. Bioelectron.*, 2011, **26**, 2246-2251.
7. L. Guo, A. R. Ferhan, K. Lee and D.-H. Kim, *Anal. Chem.*, 2011, **83**, 2605-2612.
8. C.-K. Tsung, X. Kou, Q. Shi, J. Zhang, M. H. Yeung, J. Wang and G. D. Stucky, *J. Am. Chem. Soc.*, 2006, **128**, 5352-5353.
9. J. Dintinger, S. Klein and T. W. Ebbesen, *Advanced Materials*, 2006, **18**, 1267-1270.
10. W. Ni, Z. Yang, H. Chen, L. Li and J. Wang, *J. Am. Chem. Soc.*, 2008, **130**, 6692-6693.
11. W. Ni, T. Ambjörnsson, S. P. Apell, H. Chen and J. Wang, *Nano Lett.*, 2009, **10**, 77-84.
12. S. Ye, Y. Sato and K. Uosaki, *Langmuir*, 1997, **13**, 3157-3161.
13. A. S. Viana, A. H. Jones, L. M. Abrantes and M. Kalaji, *J. Electroanal. Chem.*, 2001, **500**, 290-298.
14. X. Yao, J. Wang, F. Zhou, J. Wang and N. Tao, *J. Phys. Chem. B*, 2004, **108**, 7206-7212.
15. J. Xiang, J. Guo and F. Zhou, *Anal. Chem.*, 2006, **78**, 1418-1424.
16. H. Chen, L. Shao, Q. Li and J. Wang, *Chem. Soc. Rev.*, 2013, **42**, 2679-2724.
17. S. K. Dondapati, M. Ludemann, R. Müller, S. Schwieger, A. Schwemer, B. Händel, D. Kwiatkowski, M. Djiango, E. Runge and T. A. Klar, *Nano Lett.*, 2012, **12**, 1247-1252.